Matrix Isolated $HgCH_3$ Radical: An ESR Investigation

Emmanuel Karakyriakos and Allan J. McKinley*

Chemistry, School of Biomedical and Chemical Sciences, The University of Western Australia, 35 Stirling Highway, Crawley, Western Australia 6009

Received: January 30, 2004

The $Hg^{12}CH_3$, $Hg^{13}CH_3$, $Hg^{12}CD_3$, $^{199}Hg^{12}CH_3$, $^{201}Hg^{12}CH_3$, $^{201}Hg^{13}CH_3$, $^{199}Hg^{12}CD_3$, and $^{201}Hg^{12}CD_3$ radicals have all been formed in a microwave discharge and isolated in an inert neon matrix. Their electronic structure was established for the first time using electron spin resonance (ESR) spectroscopy. The following magnetic parameters were determined from the experimental spectra, $g_\perp = 1.84525(20)$, $A_\perp(^{199}Hg) = 4337(3)$ MHz, $A_\perp(^{201}Hg) = 1604(1)$ MHz, $A_\perp(^{13}C) = 146(2)$ MHz, $A_\perp(H) = 31(1)$ MHz, and $A_\perp(D) = 5(1)$ MHz. Estimates were made for the following magnetic parameters, $g_{||} = 1.990(5)$, $A_{||}(^{199}Hg) = 5658(10)$ MHz, $A_{||}(^{201}Hg) = 2094(10)$ MHz, and $A_{||}(^{13}C) = 270(25)$ MHz. The free atom comparison method (FACM) was used to determine the unpaired electron spin density distribution for the radical and to develop a bonding model. The $HgCH_3$ radical results are compared with our previous results for the $ZnCH_3$ and $CdCH_3$ radicals as well as other mercury-containing radicals such as HgH, HgCN, and HgF.

I. Introduction

The current investigation was prompted by our previous work on the $ZnCH_3$ and $CdCH_3$ radicals.[1,2] We now complete our study of the group 12 monomethylmetal radicals with the last of the series, the $HgCH_3$ radical. Several isotopomers of the $HgCH_3$ radical were isolated in a neon matrix and their electronic structures probed using electron spin resonance (ESR) spectroscopy. This study provides the first definitive spectroscopic observation of the $HgCH_3$ radical. The **g** tensors and a full set of magnetic hyperfine parameters are reported.

There have only been a handful of publications in the literature dealing with the $HgCH_3$ radical. The $HgCH_3$ radical is known to be one of the pyrolysis products of dimethylmercury.[3,4] The evidence thus far in the literature suggests that the mercury−carbon bond in the $HgCH_3$ radical is extremely weak. Kominar and Price investigated the thermal decomposition of dimethylmercury in a toluene carrier gas flow system and determined the mercury−carbon bond dissociation energy for the $HgCH_3$ radical to be between 1.1 and 2.6 kcal mol^{-1} with an error of ±2 kcal mol^{-1}.[5] Kallend and Purnell in another study of the gas-phase thermal decomposition of dimethylmercury suggest that the breakdown of the $HgCH_3$ radical proceeds without a measurable activation energy.[4] Jackson has applied RRKM theory combined with a steady-state master equation and determined a bond dissociation energy for the $HgCH_3$ radical of 5.4 ± 3.0 kcal mol^{-1}.[6] Therefore the $HgCH_3$ radical is expected to be an extremely unstable species.

As a result of this instability there have been few spectroscopic studies involving the $HgCH_3$ radical and there has been no definitive spectroscopic identification of this radical. The products of the photodissociation of dimethylmercury by ArF (193 nm) and KrF (248 nm) laser irradiation have been isolated in dilute argon matrixes by Crépin and co-workers.[7] The IR absorption, UV absorption, and luminescence spectra of the products were recorded. Near UV emission bands in the spectra were tentatively attributed to an unstable $Hg(^3P_0)\cdot CH_3$ complex in the matrix. An argon matrix isolation IR (MI-IR) spectroscopic study was also carried out by Snelson on the gas-phase pyrolysis products of dimethylmercury, and a tentative assignment was made for the production and trapping of the $HgCH_3$ radical.[8] Greene and co-workers have used argon matrixes to trap the products of the reaction of mercury atoms with methane.[9] The $HHgCH_3$ radical was identified as one of the products by IR spectroscopy; however, the $HgCH_3$ radical was apparently not formed even after irradiation of the matrix for 2−4 h with the output of a 500 W medium-pressure mercury arc lamp equipped with a water filter. Legay-Sommaire and Legay also formed the $HHgCH_3$ radical in an argon matrix and studied it using IR spectroscopy.[10,11] Again the $HgCH_3$ radical was not observed. An ESR study of the electron-loss centers from $HHgCH_3$ in Freon at 77 K has also been conducted.[12] The matrix was irradiated with ionizing radiation, which generated the $CH_3\cdot HgH^+$ and $CH_3Hg\cdot H^+$ radical cations. Matrix isolation studies conducted on the reactions of mercury atoms with both methane and hydrogen have identified products including HgH_2, HgD_2, HHgD, HgD, and HHgHgH in a variety of matrixes including argon, hydrogen, methane, and nitrogen.[13,14]

Mercury is a known environmental pollutant particularly in aquatic systems.[15−17] Both metallic and inorganic forms of mercury are predominantly converted to dimethylmercury in these systems through biomethylation by bacteria and fungi. The major decomposition product of dimethylmercury in aquatic systems is the water-soluble $HgCH_3^+$ cation. In fact, in living tissue most of the mercury is present as $HgCH_3^+$.[16] This compound of mercury is more toxic than the metallic form, and it is $HgCH_3^+$ that is of concern in terms of pollution control. The $HgCH_3^+$ cation bioaccumulates in organisms and is biomagnified up the food chain all the way to man.[15] Although here we are investigating the neutral radical, $HgCH_3$, the electronic structure information derived will help to elucidate the bonding and therefore properties of the $HgCH_3^+$ cation.

The matrix isolation ESR (MI-ESR) technique has already been used to study several mercury-containing species. Knight

* Corresponding author. Fax: +61-8-93801005. E-mail: ajm@chem.uwa.edu.au.

10.1021/jp0400925 CCC: $27.50
Published on Web 04/30/2004

and Weltner have isolated the HgH radical in an argon matrix and determined the **g** tensors and hyperfine structure constants for the interaction with the H, D, ^{199}Hg, and ^{201}Hg nuclei.[18] More recently, Stowe and Knight reinvestigated the electronic structure of the isotopomers of the HgH radical in both argon and neon matrixes at 4 K using MI-ESR.[19] In this study the parallel peaks of the HgH radical, which had not been observed in the earlier argon experiments, were recorded and analyzed and a full set of hyperfine and **g** tensors were determined. In the present investigation we have employed the same generation method for the $HgCH_3$ radical as that of Stowe and Knight for their study of the HgH radical. Knight and Lin have formed and trapped the HgCN radical in rare gas matrixes. The **g** tensors and hyperfine structure constants were determined by ESR for both the ^{199}Hg and ^{201}Hg isotopic forms of the radical.[20] Knight and co-workers generated the HgF radical through photolysis and isolated it in an argon matrix at 12 K.[21] The magnetic parameters obtained were used to determine the electronic structure of the radical. The MI-ESR technique has already been used to study several monomethylmetal radicals thus far. The $MgCH_3$,[22] $ZnCH_3$ [2], $CdCH_3$,[1] and $PdCH_3$[23] radicals have all been investigated using MI-ESR. Related radicals that have been investigated using this technique include $HGaCH_3$,[24] $HCuCH_3$,[25] $HAlCH_3$,[26] $FCuCH_3$,[27] and $CuCH_2$.[28]

II. Experimental Section

The main vacuum system and apparatus used for these experiments have been described in detail elsewhere.[1] A brief description of the experimental procedure specifically employed for these experiments and the modifications made to carry out these experiments will be given here.

The $HgCH_3$ radical was generated by passing mercury vapor and a methyl precursor through a microwave powered resonance lamp. The microwave source employed was a Minato Model MT-150 modified to give a full wave output coupled to an Evenson model cavity (Opthos Instruments, Inc.). The products of the gas-phase reactions were then trapped in a solid neon matrix at 4.3 K and their ESR spectra recorded. The methyl radical precursors used were $(^{12}CH_3)_3Al$ (Aldrich), $^{12}CH_3I$ (Aldrich), $^{13}CH_3I$ (Aldrich, 99 at. % ^{13}C) and $^{12}CD_3I$ (Aldrich, 99.5+ at. % D). The precursors were freeze−pump−thawed several times to remove any dissolved air but were otherwise used as received. Neon (Spectra Gases Research Grade) was passed through liquid nitrogen cooled molecular sieve traps (Linde 5A) before use. The reagent gas mixtures were prepared in a separate high-vacuum preparation system using the pressure ratios (MKS Baratron) of the neon and the specific methyl radical precursor. Typical concentrations for the $^{12}CH_3I$ and $(^{12}CH_3)_3Al$ mixtures were ≈200 ppm and ≈600 ppm for the $^{13}CH_3I$ and $^{12}CD_3I$ mixtures. The background pressure in the high-vacuum preparation system before the mixtures were made was typically 5×10^{-6} Torr. The mercury used was purified in an ultrasonic bath by washing with soapy water, 2 M nitric acid, deionized water, and then ethanol. The mercury was then transferred into a cell equipped with a Teflon stopcock and freeze−pump−thawed several times before use. The mercury vapor and the methyl radical precursor/neon gas mixture were then simultaneously passed through a 6 mm o.d. quartz tube that passed through the microwave-powered resonance lamp. On average the flow rate of the methyl radical precursor/neon gas mixture was ≈8 standard cubic centimeters per minute (sccm). The mercury flow rate was solely determined by the vapor pressure of the liquid and no additional adjustments were made. The background pressure of the main vacuum system was typically 1×10^{-7} Torr. This pressure increased to approximately 4×10^{-5} Torr with the introduction of the mercury vapor and reagent gas mixture. The matrix was deposited onto an oxygen free high-conductivity (OFHC) copper deposition target which was maintained at 4.3 K by a continuous-flow liquid helium cryostat (Cryo Industries of America RC110). The matrixes were deposited over a 1 h period. ESR spectra were recorded at temperatures of 4.3 and 9 K with a microwave power of 5 mW and a microwave frequency of approximately 9710 MHz on a Bruker ESP300E spectrometer equipped with a DM4116 cavity.

Spectral analysis was carried out on the 9 K spectra using exact diagonalization of the spin Hamiltonian with the program GEN developed by Knight and co-workers.[29,30] The spin Hamiltonian used was

$$\hat{H} = \beta_e \bar{B}\cdot\hat{g}\cdot\bar{S} + \sum_i (\bar{I}^i\cdot\hat{A}^i\cdot\bar{S} - g_n^i\beta_n\bar{B}\cdot\bar{I}^i + \bar{I}^i\cdot\hat{P}\cdot\bar{I}^i)$$

where all symbols have their usual meaning.[31] A quadrupole coupling term was included to fit the $^{201}Hg^{12}CH_3$ data. The ESR analysis was carried out using a Dec Alpha DS10 workstation. The experimental A_{iso} and A_{dip} values were derived from the following standard expressions:[31]

$$A_{iso} = \frac{2A_\perp + A_{||}}{3}$$

$$A_{dip} = A_{iso} - A_\perp$$

where

$$A_{iso} = 8\pi g_e g_n \beta_e \beta_n |\psi(0)^2|/3$$

$$A_{dip} = g_e g_n \beta_e \beta_n \langle(3\cos^2\theta - 1)/2r^3\rangle$$

III. Results

The natural isotopic distribution of mercury metal is ^{196}Hg (0.15%), ^{198}Hg (9.97%), ^{199}Hg (16.87%), ^{200}Hg (23.10%), ^{201}Hg (13.18%),^{202}Hg (29.86%), and ^{204}Hg (6.87%).[32] The only nuclei with a nonzero nuclear spin are the ^{199}Hg ($\mu = 0.50271$, $I = {}^1/_2$) and ^{201}Hg ($\mu = -0.55671$, $I = {}^3/_2$) isotopes. Therefore only radicals with these isotopes of mercury will show any metal hyperfine splitting. The other even-numbered isotopes all have no net nuclear spin ($I = 0$) and therefore will produce single overlapping ESR spectra. These isotopes will simply be designated as Hg with no specific isotopic label.

Figure 1 shows the ESR spectrum assigned to the $Hg^{12}CH_3$ radical isolated in a neon matrix at 9 K formed by passing mercury vapor and an ≈200 ppm $(^{12}CH_3)_3Al$/neon gas mixture through a microwave discharge. The upper trace shows the peaks assigned to this radical whereas the lower expanded trace provides a more detailed view of the peaks. The three equivalent hydrogen nuclei ($I = {}^1/_2$) in the radical are expected to give a quartet with a 1:3:3:1 relative intensity pattern. The peaks observed are upfield of g_e and have an approximately 1:3:3:1 relative intensity pattern and a "phase-down" line shape. This line shape suggests that these peaks are the perpendicular peaks arising from radicals with a perpendicular orientation with respect to the applied field and thus implies axial symmetry for the $HgCH_3$ radical. The parallel peaks are expected to be significantly weaker than the perpendicular peaks and were not observed in these experiments. The peaks due to the HgH and H radical species can also be seen in the upper trace of Figure 1. The lower expanded trace shows that the $HgCH_3$ radical

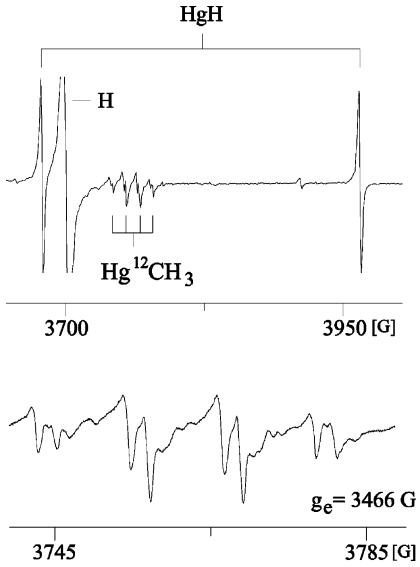

Figure 1. ESR spectrum assigned to the $Hg^{12}CH_3$ radical in a neon matrix at 9 K (upper trace) and an expanded view (lower trace). The ESR peaks due to HgH and H are also labeled.

TABLE 1: Magnetic Parameters (MHz) of the Isotopomers of the $HgCH_3$ Radical[a]

	$g_\perp$	$g_\parallel$	$A_\perp$	$A_\parallel$	A_{iso}[b]	A_{dip}[b]	Q'[c]
^{199}Hg	1.84525(20)	1.990(5)	4337(3)	5658(10)	4921(5)	345(8)	
^{201}Hg	1.84525(20)	1.990(5)	1604(1)	2094(10)	1824(4)	132(5)	98(8)
^{13}C	1.84472(20)	1.990(5)	146(2)	270(25)	188(9)	41(11)	
H[d]	1.84525(20)	1.990(5)	31(1)		31(1)		
D[d]	1.83947(20)	1.991(10)	5(1)		5(1)		

[a] The experimental uncertainties were determined by the change required to shift the simulated line positions outside the experimental line position error margin or the change required to significantly alter the simulated line shape. [b] A_{iso} and A_{dip} were calculated from standard expressions[31] and include a correction for L · I effects. These experiments cannot determine the signs of A_{iso} or A_{dip}. [c] $Q' = 3P_z/2$; see text. [d] A_{dip} for hydrogen and deuterium is expected to be small therefore A_{iso} is assumed to be equal to $A_\perp$.

occupies two major trapping sites in the matrix. The magnetic parameters given in Table 1 were determined for the predominant site using an exact diagonalization of the spin Hamiltonian to fit the experimental line positions within their experimental uncertainty. Very similar spectra were obtained using $^{12}CH_3I$ instead of $(^{12}CH_3)_3Al$. It is not clear whether the $HgCH_3$ radical is formed in the gas phase and isolated during deposition or whether the radical forms at the gas−solid interface as the neon condenses. Given the weakness of the Hg−C bond the latter appears more likely.

Figure 2 gives the ESR spectra for the $Hg^{13}CH_3$ (center trace) and $Hg^{12}CD_3$ (lower trace) radicals. The radicals were formed by passing mercury metal vapor and either a $^{13}CH_3I$/neon or a $^{12}CD_3I$/neon gas mixture through the microwave discharge. The incorporation of a ^{13}C nucleus ($I = {}^1/_2$) into the radical splits the original quartet into a pair of quartets. These peaks can be seen in the center trace of Figure 2. The lowest field peak of the lower field quartet was obscured by a larger background peak and was not observed. Each of these peaks is split in a manner similar to the unlabeled case, which is shown in the upper trace for reference. This splitting was attributed to site effects in the matrix. The spectral analysis was carried out on the predominant site. The lower trace gives the ESR spectrum for the $Hg^{12}CD_3$ radical. The three equivalent deuterium nuclei are expected to produce a septet with a relative intensity ratio of 1:6:15:20:15:6:1, which should be approximately centered

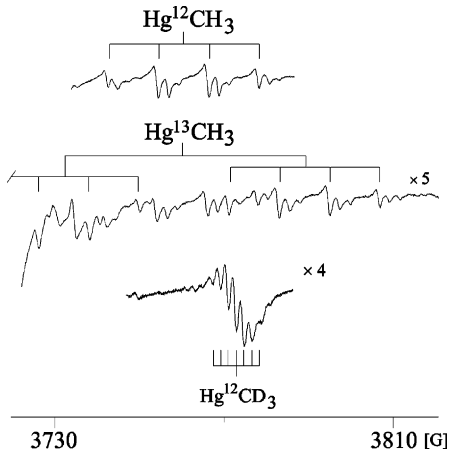

Figure 2. ESR spectra assigned to the $Hg^{13}CH_3$ (center trace) and $Hg^{12}CD_3$ (lower trace) radicals in a neon matrix at 9 K. The upper trace shows the $Hg^{12}CH_3$ radical spectrum for comparison.

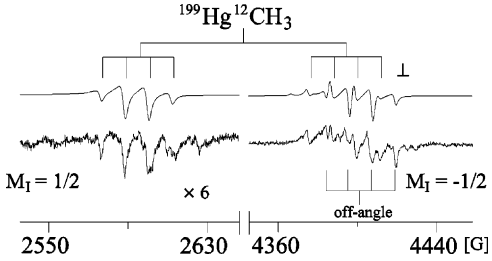

Figure 3. ESR spectrum assigned to the $^{199}Hg^{12}CH_3$ radical in a neon matrix at 9 K (lower trace). The upper trace shows the simulated ESR spectrum generated using the magnetic parameters in Table 1 (see text). The perpendicular (⊥) and off-angle peaks are labeled.

at the same field as the $Hg^{12}CH_3$ radical quartet. The partially resolved septet can be seen in the lower trace of Figure 2. The deuterium splitting is smaller than the hydrogen splitting because of the reduced magnetic moment of the deuterium nucleus compared with the hydrogen nucleus. The observed deuterium/hydrogen hyperfine splitting ratio of 0.160 is quite close to the expected ratio of 0.154 calculated from the magnetic moments of the deuterium and hydrogen nuclei. Also note that the $g_\perp$ for the $Hg^{12}CD_3$ radical is lower than the $Hg^{12}CH_3$ radical $g_\perp$ value in Table 1. This same lowering of $g_\perp$ was also observed for the HgH/HgD radical case.[18,19] The $Hg^{12}CH_3$ radical was formed in both the $Hg^{13}CH_3$ and $Hg^{12}CD_3$ experiments as an impurity species due to the presence of a background methyl source in the system. This was the case for all of the spectra recorded.

The ^{199}Hg ($I = {}^1/_2$) nucleus in the $^{199}Hg^{12}CH_3$ radical is expected to split the quartet seen in Figure 1 into a pair of widely spaced quartets. The peaks due to the $^{199}Hg^{12}CH_3$ radical are shown in the lower trace of Figure 3. The $M_I = {}^1/_2$ quartet can clearly be seen; however, the $M_I = -{}^1/_2$ quartet is not as easily distinguishable. For certain randomly orientated molecules an off-angle or off-principal-axis transition occurs when the first derivative of the ESR absorption curve is significant at an angle θ other than 0° (parallel) or 90° (perpendicular), where θ is the angle between the principal axis of the molecule and the externally applied magnetic field vector.[31,33,34] The $^{199}Hg^{12}CH_3$ radical $M_I = -{}^1/_2$ quartet is partially overlapped by an off-angle quartet, and blank experiments without mercury metal present showed small background impurity signals were underlying both these quartets. The overlap of all three of these signals, the perpendicular, off-angle, and impurity set of peaks, gives the resulting pattern seen in the lower trace of Figure 3. The top trace of this figure gives the simulated spectrum from

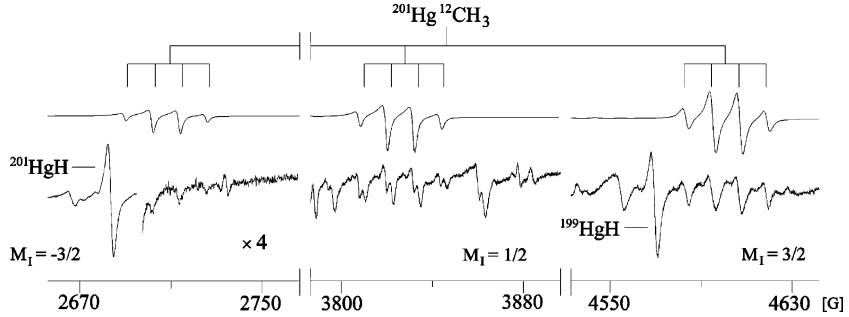

Figure 4. ESR spectrum assigned to the $^{201}Hg^{12}CH_3$ radical in a neon matrix at 9 K (lower trace). The upper trace shows the simulated ESR spectrum using the appropriate magnetic parameters in Table 1. The $M_I = -1/2$ quartet was obscured by the low-field H line (see text). The $^{199/201}HgH$ radical peaks occurring in this field region are been labeled.

an exact diagonalization of the spin Hamiltonian using the magnetic parameters in Table 1. The magnetic parameters given in Table 1 were determined by fitting the observed peak positions and matching the correct line shape and relative intensities. The uncertainties in the fitted parameters were estimated by varying each value until either the simulated peak positions were outside the experimental uncertainty or the line shape was significantly altered from the experimentally observed line shape. Although the parallel peaks were not observed, estimates could be made for the $g_{||}$ and $A_{||}$ values through their effect on the perpendicular peaks and the off-angle set of peaks that were particularly sensitive to these values. The signs of the hyperfine coupling parameters cannot be determined by these experiments. The magnetic hyperfine parameters given in Table 1 are for the major matrix site. The simulated peaks for the $^{199}Hg^{12}CH_3$ radical show a good match with line position, line shape, and the relative intensities between the $M_I = +1/2$ and $-1/2$ set of peaks. The only discrepancy is the relative intensities of the peaks for the off-angle quartet for the $M_I = -1/2$ set of peaks. However, it is quite likely that the overlap of the off-angle peaks with the background contaminant peaks that were present in this region as well as the perpendicular peaks would change the relative intensities of the peaks from those observed in the simulation.

The lower trace of Figure 4 shows the peaks observed for the $^{201}Hg^{12}CH_3$ radical. The ^{201}Hg nucleus ($I = 3/2$) is expected to give four widely spaced quartets. The $M_I = -3/2$, $+1/2$, and $+3/2$ quartets were all observed; unfortunately, the $M_I = -1/2$ quartet was totally obscured by the low-field hydrogen atom peak and could not be observed. Peaks from the ^{199}HgH and ^{201}HgH radicals are also labeled in this figure. In fact, one of the ^{201}HgH radical peaks partially obscures the $M_I = -3/2$ quartet. The upper trace of Figure 4 gives the simulated $^{201}Hg^{12}CH_3$ radical spectrum using the magnetic parameters in Table 1 and an exact diagonalization of the spin Hamiltonian. The simulated peaks show a good match with the experimental peak positions, peak shape, and relative intensities between the $M_I = -3/2$, $+1/2$, and $+3/2$ quartets. A quadrupole term had to be introduced into the spin Hamiltonian to obtain a reasonable fit with the experimental spectrum; this value ($Q' = 3P_z/2$) is given in Table 1. The $M_I = 3/2$ peaks appear slightly broader than the other sets due to the overlap of an off-angle quartet with the perpendicular quartet. The $M_I = 1/2$ quartet shows the presence of a second site which was not as intense for the $M_I = -3/2$ and $+3/2$ sets of peaks. It was found during the course of these experiments that using a CH_3I methyl precursor rather than $(CH_3)_3Al$ results in a less significant site effect. Even though a second site was present in some of the spectra recorded where a CH_3I precursor was used, it was always substantially smaller than in the $(CH_3)_3Al$ case. This reduced signal intensity

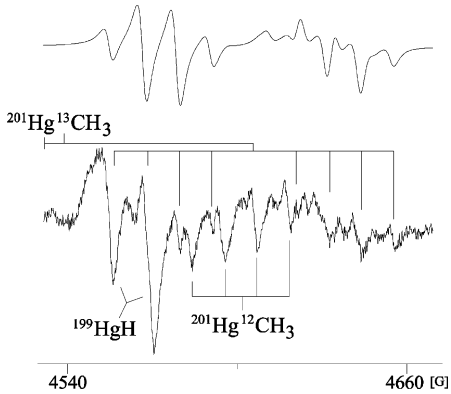

Figure 5. ESR spectrum of the $M_I = 3/2$ $^{201}Hg^{13}CH_3$ radical in a neon matrix at 9 K (lower trace). The upper trace shows the corresponding simulated ESR spectrum using the appropriate parameters in Table 1. Peaks due to the $^{201}Hg^{12}CH_3$ and ^{199}HgH radicals are also labeled.

for one of the sites using the $(CH_3)_3Al$ precursor allowed the identification of the peaks belonging to a particular matrix site.

Figure 5 shows the peaks due to the ^{13}C splitting of the $M_I = 3/2$ $^{201}Hg^{13}CH_3$ radical. The $A_{||}(^{13}C)$ value does not have a significant effect on the $Hg^{13}CH_3$ radical peak positions. Therefore the determination of the $A_{||}(^{13}C)$ value for the ^{13}C nucleus was carried out using the $M_I = 3/2$ $^{201}Hg^{13}CH_3$ radical spectrum shown in the lower trace of Figure 5. Two of the peaks of the lower field quartet are obscured due to significantly more intense peaks associated with the ^{199}HgH radical; background $^{201}Hg^{12}CH_3$ radical peaks are also present. The higher field set of peaks in the spectrum are a combination of the perpendicular and off-angle quartets. The off-angle quartet is more intense than the perpendicular quartet it overlaps with and is more sensitive to changes of the $A_{||}(^{13}C)$ value than the perpendicular peaks. This allows us to make a better estimate for the $A_{||}(^{13}C)$ value, although we still have a relatively large associated uncertainty. The upper trace of Figure 5 is the simulated spectrum for this region using the relevant magnetic parameters in Table 1. A relatively good fit between the simulated and experimental spectra is obtained. The experimental off-angle peaks are slightly broader than the simulated off-angle peaks.

Figure 6 shows the θ versus magnetic field plots superimposed on the simulated ESR spectra for the $^{199}Hg^{12}CH_3$, $^{201}Hg^{12}CH_3$, and $^{201}Hg^{13}CH_3$ radicals. The experimental spectra are also included for comparison. From this figure we are able to differentiate the off-angle peaks from the perpendicular set of peaks. As mentioned previously, we do not observe the significantly weaker parallel set of peaks. For the $^{201}Hg^{12}CH_3$ radical peaks and the lower field set of peaks of the $^{201}Hg^{13}CH_3$ radical the off-angle and perpendicular peaks completely overlap and remain unresolved.

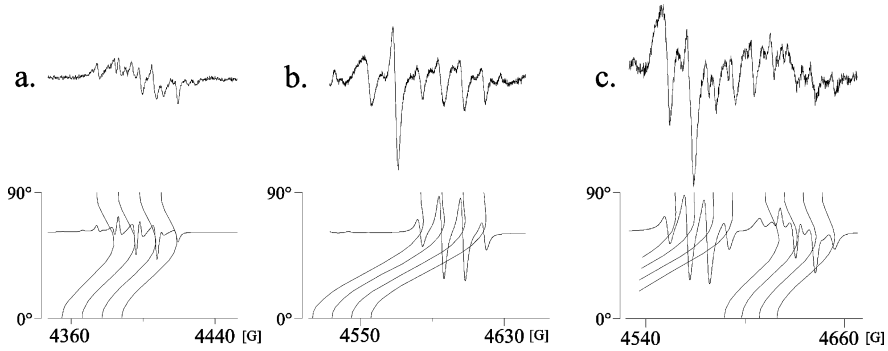

Figure 6. θ versus field (G) plots superimposed on the simulated ESR spectra of (a) $^{199}Hg^{12}CH_3$ $M_I = -1/2$, (b) $^{201}Hg^{12}CH_3$ $M_I = 3/2$, and (c) $^{201}Hg^{13}CH_3$ $M_I = 3/2$. The experimental ESR spectra are also given for each of the radicals (upper trace).

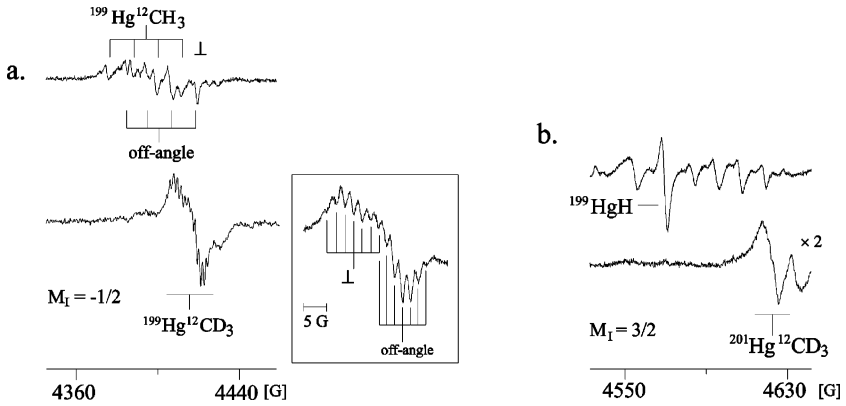

Figure 7. (a) ESR spectrum assigned to the $M_I = -1/2$ $^{199}Hg^{12}CD_3$ radical in a neon matrix at 9 K (lower trace). The inset shows an expanded view of these peaks and labels the perpendicular (⊥) and off-angle sets of peaks. The upper trace gives the $M_I = -1/2$ $^{199}Hg^{12}CH_3$ radical set of peaks for comparison. (b) ESR spectrum assigned to the $M_I = 3/2$ $^{201}Hg^{12}CD_3$ radical in a neon matrix at 9 K (lower trace). The $M_I = 3/2$ $^{201}Hg^{12}CH_3$ radical ESR spectrum is given in the upper trace for comparison.

Figures 7 shows the effect of deuteration on the most intense metal hyperfine peaks for the $^{199}Hg^{12}CD_3$ and $^{201}Hg^{12}CD_3$ radicals. The $^{199}Hg^{12}CH_3$ and $^{201}Hg^{12}CH_3$ radical peaks in this region are also given for comparison. As explained previously for the $Hg^{12}CD_3$ radical septet, the deuterium hyperfine splitting is smaller than the hydrogen hyperfine splitting. The ratio of the deuterium and hydrogen splitting agrees with that expected from the ratio of the deuterium and hydrogen magnetic moments. The lower trace of Figure 7a shows the two sets of septets due to both the perpendicular and off-angle transitions for the $M_I = -1/2$ $^{199}Hg^{12}CD_3$ radical set of peaks. The lower trace of Figure 7b gives the $^{201}Hg^{12}CD_3$ radical spectrum for the $M_I = 3/2$ field region. Due to the lower intensity of these peaks compared with the $^{199}Hg^{12}CD_3$ set of peaks, a higher amplitude modulation had to be used, and as a result, the septet remained unresolved and we see only a single broad feature.

IV. Discussion

The electron spin density distribution for the $HgCH_3$ radical was determined using the free atom comparison method (FACM). This method involves taking the ratio of the molecular A_{iso} and A_{dip} for each nucleus in the radical with their respective atomic values. The FACM approximation neglects core polarization, overlap effects, and hyperfine contributions from orbitals centered on other atoms in the molecule. The values obtained are the respective spin densities. A linear combination of atomic orbitals (molecular orbitals) or LCAO-MO model for the HOMO of the $HgCH_3$ radical would take the following form:

$$\Psi(X^2A_1) = a_1\chi(\text{Hg 6s}) + a_2\chi(\text{Hg 6p}) + a_3\chi(\text{C 2s}) + a_4\chi(\text{C 2p}) + a_5\chi(\text{H 1s})$$

where $\Psi(X^2A_1)$ is the molecular wave function of the HOMO. The atomic orbitals are represented by the χ(Hg 6s), etc. terms, and the a_1, etc. factors represent the coefficients for the atomic orbital contribution to the HOMO. The FACM values provide the squares of these values. Standard theoretical atomic A_{iso} and A_{dip} values were used for both the carbon and hydrogen nuclei.[31] The ^{199}Hg and ^{201}Hg atomic A_{iso} and A_{dip} values were determined from the hyperfine coupling constants a_s, $a_{1/2}$, and $a_{3/2}$, which have been derived from atomic-beam magnetic resonance experiments.[35] Although $a_{1/2}$ was not directly determined in these atomic-beam experiments, it can be determined from the $a_{3/2}$ value and the following theoretical relationship:[35]

$$a_{1/2} = 5\theta(1-\delta)_{1/2}(1-\epsilon)_{1/2}a_{3/2}$$

The relativistic correction factor used θ was taken from Schwartz.[36] The a_s value is the equivalent of the A_{iso}, value and the atomic A_{dip} value can be derived from the $a_{1/2}$ and $a_{3/2}$ values using the following equations:[37]

$$\bar{P} = {}^5/_{16}(a_{1/2} + a_{3/2})$$

$$A_{dip} = {}^2/_5\bar{P}$$

The above equations are approximations and do not include any relativistic corrections. The atomic parameters determined were as follows: $A_{iso}(^{199}Hg)$ = 35110(80) MHz, $A_{dip}(^{199}Hg)$ = 611(42) MHz, $A_{iso}(^{201}Hg)$ = 12980(30) MHz, and $A_{dip}(^{201}Hg)$ = 225(16) MHz.

Table 2 shows the results of the FACM analysis on the hyperfine data in Table 1 for the $HgCH_3$ radical. The HOMO is predominantly mercury 6p orbital in character with a smaller

TABLE 2: Comparison of the Experimental Spin Densities[a] for the $HgCH_3$, $CdCH_3$ and $ZnCH_3$ Radicals

	$^{199}Hg/^{201}Hg/^{111}Cd/^{67}Zn$		^{13}C		H	total
	$a_1^2\chi$(ns)	$a_2^2\chi$(np$_z$)	$a_3^2\chi$(ns)	$a_4^2\chi$(np$_z$)	$a_5^2\chi$(ns)	$\Sigma_{i=1}^5 a_i^2$
$^{199}HgCH_3$[b]	0.14(1)	0.56(6)	0.05(1)	0.38(10)	0.02(1)	1.2(2)
$CdCH_3$[c]	0.26(1)	0.45(10)	0.05(9)	0.16(16)	−0.01(6)	0.89(33)
$ZnCH_3$[d]	0.29(1)	0.56(20)	0.05(10)	0.13(20)	−0.01(7)	1.0(6)

[a] The experimental values were determined using the free atom comparison method (FACM); see text. The errors are the larger of either ±0.01 or the standard propagated error based on the A_{iso} and A_{dip} experimental errors. The FACM values are only given for the Hg-199 isotope of $HgCH_3$. The Hg-201 FACM values are within the experimental error margins given above. [b] This work. [c] From refs 1 and 2. [d] From ref 2.

TABLE 3: Comparison of the Magnetic Parameters (MHz) and Experimental Spin Densities[a] for Various Mercury-Containing Radicals

	$A_{iso}(^{199}Hg)$	$A_{dip}(^{199}Hg)$	$a_1^2\chi$(6s)	$a_2^2\chi$(6p$_z$)
$^{199}HgCH_3$[b]	4921(5)	345(8)	0.14(1)	0.56(10)
^{199}HgH[c]	6859(3)	446(3)	0.20(1)	0.73(1)
$^{199}HgCN$[d]	15960(20)	396(15)	0.45(1)	0.65(11)
^{199}HgF[e]	22163(12)	223(8)	0.63(1)	0.36(11)

[a] The experimental values were determined using the free atom comparison method, (FACM) and atomic vales of $A_{iso}(^{199}Hg)$ = 35110(80) MHz and $A_{dip}(^{199}Hg)$ = 611(42) MHz. The errors are the larger of either ±0.01 or the standard propagated error based on the A_{iso} and A_{dip} experimental errors. [b] This work. [c] The spin densities were derived from the A_{iso} and A_{dip} values given in ref 19. [d] The spin densities were derived from the A_{iso} and A_{dip} values given in ref 20. [e] The spin densities were derived from the A_{iso} and A_{dip} values given in ref 21.

mercury 6s orbital contribution. The remaining spin density is on the carbon nucleus in a 2p orbital. The total spin density on the carbon nucleus is higher than that observed for the previously studied $CdCH_3$ and $ZnCH_3$ radicals and could be due to the mercury atom having the highest ionization energy of the group 12 elements. This means the two mercury valence electrons are more tightly bound to the nucleus, which would lead to an overall reduction in the unpaired electron spin density on the mercury nucleus and a corresponding increase for the carbon nucleus. One of the main differences between the $HgCH_3$ radical and the $CdCH_3$ and $ZnCH_3$ radicals is the reduced metal s orbital character of the HOMO. This is indicative of a metal−carbon bond with covalent greater than ionic character. The metal p orbital characters for all three of these radicals do not differ significantly; however, the unpaired electron spin density of the metal s orbital has shifted onto the methyl group in the $HgCH_3$ radical. This brings us to the second major difference between the $HgCH_3$ radical and the $ZnCH_3$ and $CdCH_3$ radicals. The carbon 2p orbital character is significantly higher for the $HgCH_3$ radical compared to the two previously investigated group 12 monomethylmetals. The carbon 2s characters are small and equal within experimental error for all three radicals. It is interesting that the $HgCH_3$ radical has the lowest metal s orbital character in its HOMO and the lowest bond energy when compared with the $CdCH_3$ and $ZnCH_3$ radicals. This would suggest that the lower the contribution of the metal s orbital in the HOMO the lower the metal−carbon bond strength. For a purely ionic bond we would expect the unpaired electron to be almost entirely localized in the mercury 6s orbital with negligible mercury 6p character. For a purely covalent bond assuming sp hybridization on the mercury, we would expect approximately 50% mercury 6p character. The relatively high mercury 6p orbital character and relatively low mercury 6s orbital character of the HOMO would seem to suggest that the mercury−carbon bonding in the radical is more covalent than ionic in nature.

Jackson[6] proposed a qualitative molecular orbital diagram for $ZnCH_3$ with the metal carbon bonding being a doubly occupied σ orbital and a singly occupied σ^* orbital. These orbitals arise from the overlap of the methyl sp^3 orbital and a mixture of metal valence s and p orbitals. The large difference between the FACM derived populations in the metal s and p orbital in the $HgCH_3$ radical HOMO compared with the $ZnCH_3$ and $CdCH_3$ radical cases can also be attributed to an uneven contribution of these atomic orbitals to the σ and σ^* molecular orbitals. The atomic mercury 6s and 6p orbitals have a significantly larger energy difference between them than the corresponding 4s and 4p orbitals of zinc and the 5s and 5p orbitals of cadmium. Therefore the bonding σ molecular orbital should have a greater proportion of the lower energy atomic orbital, i.e., s orbital, and the higher energy σ^* molecular orbital (HOMO) should have a higher proportion of the higher energy atomic orbital, i.e., p orbital. This was observed for both the $CdCH_3$ and $ZnCH_3$ radicals, and it is the case here for the $HgCH_3$ radical, except that we see a larger difference between the mercury s and p orbital characters due to the aforementioned larger energy difference between the atomic mercury 6s and 6p orbitals.

The $g_\perp$ value decreases as we go from $ZnCH_3$ to $CdCH_3$ to $HgCH_3$. The greatest deviation from g_e is observed for the $HgCH_3$ radical. The deviation of $g_\perp$ from g_e, $\Delta g_\perp$, can be estimated by the following relationship, $\Delta g_\perp = g_\perp - g_e = -2\zeta a_2/\Delta E$,[20] where ζ is the metal spin−orbit coupling constant, a_2 is the metal p orbital character of the HOMO, and ΔE is the energy separation between the ground and first excited states. Because the mercury atom has a larger spin−orbit coupling constant than cadmium and zinc and the a_2 values are very similar for all three radicals, the $\Delta g_\perp$ value for the $HgCH_3$ radical is expected to be the greatest overall.

In previous cases both the $CdCH_3$ and $ZnCH_3$ radicals have had bonding and electronic structures similar to those of their respective hydrides and to each other. The FACM values for the $HgCH_3$/HgH radical pair (Table 3) show the same trends observed for the $CdCH_3$/CdH and $ZnCH_3$/ZnH radical cases; i.e., metal s orbital character increases and metal p orbital character remains relatively unchanged within experimental error between the monomethyl and hydride radicals. Overall, the FACM values show a similar spin density distribution for the $HgCH_3$ and HgH radicals, with most of the unpaired electron spin density on the mercury. The spin density analysis for the HgH radical was carried out using values from the latest HgH study of Stowe and Knight.[19] In an earlier investigation of the HgH radical the weaker parallel peaks were not observed and so the mercury $A_{||}$ value could only be estimated from its effect on the perpendicular peaks. In the latter investigation the parallel peaks were observed; therefore the mercury $A_{||}$ value and thus the mercury A_{dip} value could be measured directly. The radical was also trapped in neon, giving us a better overall comparison between the HgH radical and the neon matrix isolated $HgCH_3$ radical. Using the FACM, a 0.73 value is obtained for the mercury 6p orbital character. Stowe and Knight suggest some uncertainty in the appropriate value for the atomic mercury A_{dip} value and that perhaps the actual value should be higher, which would give a smaller mercury 6p orbital character. This value does not correspond well with that obtained for the mercury 6p orbital character in the $HgCH_3$ radical. Another method of estimating the mercury 6p orbital character in the HgH HOMO is by using the aforementioned $\Delta g_\perp$ equation. Using the $g_\perp$ for the HgH radical in neon of 1.8113,[19] ΔE value of 24 934 cm^{-1},[38] and a ζ_{6p} value of ∼4150 cm^{-1},[39] the estimated a_2 value is 0.57. This value is remarkably close to our FACM-derived a_2 value

of 0.56(6) for the $HgCH_3$ radical. Using this approach to estimate a_2 for the $HgCH_3$ radical given that the $g_\perp$ value in neon is 1.8453 and assuming the same ΔE value as for HgH of 24 934 cm^{-1}, we obtain a value for a_2 of 0.47. In addition, we can estimate the a_2 value for the $HgCH_3$ radical from the Hg-201 quadrupole coupling constant $|Q'|$ if we assume the Hg−C bond has largely σ character and is purely covalent and that the mercury d orbitals are not involved in the bonding. The measured value of $|Q'|$ can be related[40] to the molecular term $|3eqQ|_{mol}$, where $|Q'| = |3eqQ|_{mol}/4I(2I - 1)$ and where q is the electric field gradient along the Hg−C bond, Q is the nuclear quadrupole moment, and for Hg-201 $I = {}^3/_2$. Using our measured value of 98(8) MHz for $|Q'|$, we obtain $|eqQ|_{mol} = 392$ MHz for the $HgCH_3$ radical, which, when divided by the atomic value[41] of $|eqQ|_{atom} = 780$ MHz, gives $a_2 = 0.50$, which is again consistent with the other derivations. The monomethyl-metals and metal hydrides of zinc and cadmium also showed extremely similar a_2 values.

The $g_\perp$ values for the previously investigated metal methyl and metal hydride radicals were very similar. This does not seem to be the case for the $HgCH_3$ and HgH radicals. The $g_\perp$ values deviate by a greater amount than in the $CdCH_3$/CdH and $ZnCH_3$/ZnH radical cases. The $HgCH_3$ radical $g_\perp$ value may deviate from the HgH radical $g_\perp$ value if we have isolated a $Hg{\cdot}CH_3$ complex rather than the $HgCH_3$ radical. Crépin and co-workers formed what they believed to be a $Hg(^3P_0){\cdot}CH_3$ complex in an argon matrix during the photodissociation of dimethylmercury.[7] A structured 338 nm emission was observed, and the species responsible was thought to be either the $HgCH_3$ radical, a strongly bonded complex such as $Hg{\cdot}C_2H_4$, $Hg{\cdot}C_2H_4$, or $Hg(^3P_0){\cdot}CH_3$, or dimethylmercury itself. Crépin and co-workers believed the species most likely for this structured emission was the $Hg(^3P_0){\cdot}CH_3$ complex. The reasons they assigned the complex rather than the radical are as follows: significantly different ΔE value when compared to the $CdCH_3$, $ZnCH_3$, and HgH radicals and a long decay time (∼4 ms) for the emission that is characteristic of $Hg(^3P_0)$ complexes and not of MCH_3 radicals (M = metal) However, they could only give a tentative assignment as the large Stokes shift, the vibrational spacings, and the decreasing intensity of the emission with photolysis time indicated that the assignment was far from definitive. Given that the excited state species observed by Crépin and co-workers has a lifetime of the order of milliseconds, we would only be able to observe the corresponding ground-state species, $Hg(^1S_0){\cdot}CH_3$, in our experiments. Our ESR results are not consistent with a $Hg(^3P_0){\cdot}CH_3$ or a $Hg(^1S_0){\cdot}CH_3$ complex. The species we observe has a doublet ground state. We would expect the $Hg(^3P_0){\cdot}CH_3$ complex to have a quartet ground state in line with previous matrix-isolated spin pair complexes such as H· ··H and N· ··N which are known to be high-spin systems.[42,43] The $Hg(^1S_0){\cdot}CH_3$ complex would not show the large mercury p character (approx 0.5) we observe. We believe our mercury p character value is reliable, as consistent values were obtained with three completely independent derivations, as discussed above. In addition, several methyl radical adducts have been observed by ESR spectroscopy, e.g., $CH_3{\cdot}I^-$ and $CH_3{\cdot}Br^-$.[44,45] These radicals have g values close to 2.0023, have methyl hydrogen hyperfine values close to the free methyl radical (typically about 90%), and show spin density of between 5% and 10% on the heteroatom. Such characteristics are not consistent with the radicals observed in this work. Finally, the bonding and electronic structure determined by the FACM for what we believe to be the $HgCH_3$ radical seems to agree with the general bonding trend and electronic structure determined for the other group 12 monomethyl radicals as well as the HgH radical. This leads us to believe that we have in fact trapped and formed the $HgCH_3$ radical and not the $Hg(^3P_0){\cdot}CH_3$ or $Hg(^1S_0){\cdot}CH_3$ complex. High-level ab initio calculations would help to confirm our assignment and we would encourage other workers to undertake such studies.

Table 3 gives the $A_{iso}(^{199}Hg)$ and $A_{dip}(^{199}Hg)$ values and the FACM derived mercury 6s and 6p characters for various mercury-containing radicals. The $HgCH_3$ radical has the lowest A_{iso} value and hence the lowest overall mercury 6s orbital character in the HOMO. This implies that the bonding is more covalent in nature compared with the other radicals. As we move down Table 3, the ionic nature of the bonding increases and this is reflected in the increasing $A_{iso}(^{199}Hg)$ value and therefore increasing mercury 6s orbital character. This is not surprising as the electronegativity of the substituent increases as we move down Table 3.

V. Conclusions

The various isotopomers of the $HgCH_3$ radical were formed in a microwave discharge and isolated in a neon matrix, and their electronic structures were probed for the first time using ESR spectroscopy. $g_\perp$, $A_{iso}(^{199}Hg)$, $A_{iso}(^{201}Hg)$, $A_{iso}(^{13}C)$, $A_\perp(H)$, and $A_\perp(D)$ were all derived from the ESR spectra. Estimates were determined for the $g_{||}$, $A_{dip}(^{199}Hg)$, $A_{dip}(^{201}Hg)$, and $A_{dip}(^{13}C)$ parameters. These values were used in a free atom comparison method (FACM) analysis to determine the unpaired electron spin density distribution for the radical. The unpaired electron seems to be largely localized on the mercury atom in the radical. The $HgCH_3$ radical seems to have a metal−carbon bond that has a lower ionic character than both the $ZnCH_3$ and $CdCH_3$ radicals. The $HgCH_3$ radical has the lowest overall metal s orbital character and the highest carbon 2p orbital contribution to the highest occupied molecular orbital (HOMO) of all the group 12 monomethyl radicals. It was also found to have the lowest ionic character compared with the HgH, HgCN, and HgF radicals. The FACM results for the HgH and $HgCH_3$ radicals, however, do suggest that the mercury−carbon and mercury−hydrogen bond are quite similar.

Acknowledgment. A.J.M. thanks the Australian Research Council for support of this work under the Small Grants Scheme and The Australian Government Department of Education, Employment, Training and Youth Affairs (DETYA) who provided a Research Infrastructure, Equipment and Facilities Grant that was used to purchase the ESR spectrometer at UWA. E.K. thanks DETYA for an Australian Postgraduate Award with stipend and UWA for a Jean Rogerson Postgraduate Scholarship. We both thank Dr Lon B. Knight Jr. of Furman University for helpful discussions concerning this work.

References and Notes

(1) Karakyriakos, E.; Davis, J. R.; Wilson, C. J.; Yates, S. A.; McKinley, A. J.; Knight, L. B., Jr.; Babb, R.; Tyler, D. J. *J. Chem. Phys.* **1999**, *110*, 3398.

(2) McKinley, A. J.; Karakyriakos, E.; Knight, L. B., Jr.; Babb, R.; Williams, A. *J. Phys. Chem. A* **2000**, *104*, 3528.

(3) Long, L. H. *J. Chem. Soc., Faraday Trans.* **1955**, *51*, 673.

(4) Kallend, A. S.; Purnell, J. H. *J. Chem. Soc., Faraday Trans.* **1964**, *60*, 103.

(5) Kominar, R. J.; Price, S. J. *Can. J. Chem.* **1969**, *47*, 991.

(6) Jackson, R. L. *Chem. Phys. Lett.* **1990**, *174*, 53.

(7) Crépin, C.; Legay-Sommaire, N.; McCaffrey, J. G.; Tramer, A. *J. Phys. Chem. A* **1998**, *102*, 4014.

(8) Snelson, A. *J. Phys. Chem.* **1970**, *74*, 537.

(9) Greene, T. M.; Andrews, L.; Downs, A. J. *J. Am. Chem. Soc.* **1995**, *117*, 8180.

(10) Legay-Sommaire, N.; Legay, F. *Chem. Phys. Lett.* **1994**, *217*, 97.
(11) Legay-Sommaire, N.; Legay, F. *Chem. Phys. Lett.* **1996**, *211*, 367.
(12) Almond, M. J.; Rice, D. A.; Sheridan, L. A.; Craig, P. J.; Stojak, G.; Symons, M. C. R., Rai, U. S. *J. Chem. Soc., Faraday Trans.* **1994**, *90*, 3153.
(13) Legay-Sommaire, N.; Legay, F. *Chem. Phys. Lett.* **1993**, *207*, 123.
(14) Legay-Sommaire, N.; Legay, F. *J. Phys. Chem.* **1995**, *99*, 16945.
(15) Mitra, S. *Mercury in the Ecosystem: Its Dispersion and Pollution Today*; Trans Tech Publications Ltd: Aedermannsdorf, Switzerland, 1986.
(16) Beyer, W. N., Heinz, G. H., Redmon-Norwood, A. W., Eds. *Environmental Contaminants in Wildlife: Interpreting Tissue Concentrations*; CRC Press: Boca Raton, FL, 1996.
(17) Farago, M. E. Chemical Processes in Marine Environments. In *Mercury in Marine Environments*; Gianguzza, A., Pelizzetti, E., Sammartano, S., Eds.; Springer: Berlin, 2000; Chapter 13.
(18) Knight, L. B., Jr.; Weltner, W., Jr. *J. Chem. Phys.* **1971**, *55*, 2061.
(19) Stowe, A. C.; Knight, L. B., Jr. *Mol. Phys.* **2002**, *100*, 353.
(20) Knight, L. B., Jr.; Lin, K. C. *J. Chem. Phys.* **1972**, *56*, 6044.
(21) Knight, L. B., Jr.; Fisher, T. A.; Wise, M. B. *J. Chem. Phys.* **1981**, *74*, 6009.
(22) McKinley, A. J.; Karakyriakos, E. *J. Phys. Chem. A* **2000**, *104*, 8872.
(23) Knight, L. B., Jr.; Herlong, J. O.; Cobranchi, S. T.; Kirk, T. *J. Chem. Phys.* **1990**, *92*, 6463.
(24) Knight, L. B., Jr.; Banisaukas, T. J., III; Babb, R.; Davidson, E. R. *J. Chem. Phys.* **1996**, *105*, 6607.
(25) Ozin, G. A.; McCaffrey, J. G.; Parnis, J. M. *Angew. Chem., Int. Ed. Engl.* **1986**, *25*, 1072.
(26) Parnis, J. M.; Ozin, G. A. *J. Phys. Chem.* **1989**, *93*, 1204.
(27) Knight, L. B., Jr.; Cobranchi, S. T.; Gregory, B. W.; Jones, G. C., Jr. *J. Chem. Phys.* **1988**, *88*, 524.
(28) Knight, L. B., Jr.; Cobranchi, S. T.; Petty, J.; Cobranchi, D. P. *J. Chem. Phys.* **1989**, *91*, 4587.
(29) Knight, L. B., Jr.; Steadman, J.; Miller, P. K.; Cleveland, J. A., Jr. *J. Chem. Phys.* **1988**, *88*, 2226.
(30) Knight, L. B., Jr.; Cobranchi, S. T.; Earl, E. *J. Chem. Phys.* **1988**, *88*, 7348.
(31) Weltner, W., Jr. *Magnetic Atoms and Molecules*; Dover: New York, 1989.
(32) *CRC Handbook of Chemistry & Physics*, 79th ed.; Lide, D. R., Ed.; CRC Press: Boca Raton, FL, 1998.
(33) Neiman, R.; Kivelson, D. *J. Chem. Phys.* **1961**, *35*, 156.
(34) Gersmann, H. R.; Swalen, J. D. *J. Chem. Phys.* **1962**, *36*, 3221.
(35) McDermott, M. N.; Lichten, W. L. *Phys. Rev.* **1960**, *119*, 134.
(36) Schwartz, C. *Phys. Rev.* **1957**, *105*, 173.
(37) Ammeter, J. H.; Schlosnagle, D. C. *J. Chem. Phys.* **1973**, *59*, 4784.
(38) Mayama, S.; Hiraoka, S.; Kinichi, O. *J. Chem. Phys.* **1984**, *81*, 4760.
(39) Moore, C. E. *Atomic Energy Levels*; NBS: Washington, DC, 1958; Vol. III.
(40) Van Zee, R. J.; Hamrick, Y. M.; Li, S.; Weltner, W., Jr. *J. Phys. Chem.* **1992**, *96*, 7247.
(41) Gordy, W.; Cook, R. L. *Microwave Molecular Spectra*; John Wiley: New York, 1984; p 737.
(42) Knight, L. B., Jr.; Rice, W. E.; Moore, L.; Davidson, E. R. *J. Chem. Phys.* **1995**, *103*, 5275.
(43) Knight, L. B., Jr.; Bell, B. A.; Cobranchi, D. P.; Davidson, E. R. *J. Chem. Phys.* **1999**, *111*, 3145.
(44) Sprague, E. D.; Williams, F. F. *J. Chem. Phys.* **1971**, *54*, 5425.
(45) Symons, M. C. R.; Smith, I. G. *J. Chem. Soc., Perkin Trans. 2* **1981**, 1181.